

Vitrification of CO2-mineralized steel slag residual: A study on the formulation, high-temperature viscosity-component correlation and chemical durability of glass.

LEI, Hongming, JI, Long, NIU, Chenchen, CHAKRABARTI, Anirban, DENG, Wei http://orcid.org/0000-0002-1793-8455 and XU, Kai

Available from Sheffield Hallam University Research Archive (SHURA) at:

https://shura.shu.ac.uk/36319/

This document is the Accepted Version [AM]

Citation:

LEI, Hongming, JI, Long, NIU, Chenchen, CHAKRABARTI, Anirban, DENG, Wei and XU, Kai (2025). Vitrification of CO2-mineralized steel slag residual: A study on the formulation, high-temperature viscosity-component correlation and chemical durability of glass. Construction and Building Materials, 500: 144158. [Article]

Copyright and re-use policy

See http://shura.shu.ac.uk/information.html

Vitrification of CO₂-mineralized steel slag residual: A study on the

formulation, high-temperature viscosity-component correlation and

chemical durability of glass

Hongming Lei^a, Long Ji^b, Chenchen Niu^a, Anirban Chakrabarti^a, Wei Deng^c, Kai Xu^{a,*}

^a State Key Laboratory of Silicate Materials for Architectures, Wuhan University of

Technology, Wuhan 430070, China

^b College of Engineering, Huazhong Agricultural University, Wuhan 430070, China

^c College of Business, Technology and Engineering, Sheffield Hallam University, City

Campus, Sheffield S1 1WB, UK

* Corresponding author

Abstract:

China's extensive accumulation of steel slag not only occupies significant land resources but also poses risks to soil and groundwater quality. CO2 mineralization technology presents an effective strategy for detoxifying and repurposing steel slag, simultaneously generating valuable carbonates and facilitating carbon sequestration. However, the residual material resulting from CO₂ mineralization of steel slag contains hazardous heavy metals and organic compounds, including amino acids that act as leaching agents. This study aimed to stabilize the CO2-mineralized steel slag residue through vitrification, transforming it into a stable glass matrix. Ternary glasses composed of CMSSR-SiO₂-Al₂O₃ were synthesized at a melting temperature of 1300 °C. The glass-forming region was delineated within compositional boundaries of 45-77.5 wt% CMSSR, 22.5-40 wt% SiO₂, and 0-15 wt% Al₂O₃. A representative set of formulations was selected to examine high-temperature viscosity, and a quadratic mixture model was developed to correlate component ratios with the temperature at which viscosity reaches 10 Pa·s. The leaching behavior of heavy metals was evaluated using an acid leaching protocol in accordance with Chinese national standards, with results indicating excellent chemical durability of the vitrified glasses.

Key words:

CO₂-mineralized steel slag residual, Vitrification, Glass formulation, Viscosity-component correlation, Chemical durability, Acid leaching.

1. Introduction

China's steel slag production has exceeded 120 million tons per year [1,2], and such a large accumulation of steel slag not only occupies land but also threatens the soil and groundwater [3,4]. To detoxify and repurpose steel slag, extensive research has been conducted across various industries, with CO₂ mineralization technology emerging as a prominent approach [5,6]. This method effectively addresses the challenges associated with steel slag treatment, while concurrently generating valuable carbonates and promoting CO₂ sequestration [7–9]. However, the residue produced from CO₂ mineralization of steel slag—hereafter referred to as CMSSR—contains hazardous heavy metals and organic compounds such as amino acids, which act as leaching agents. These contaminants necessitate further immobilization and removal prior to final disposal.

Vitrification has proven to be a reliable method for transforming hazardous waste into chemically durable glassy materials [10,11]. This process involves melting the waste in combination with glass-forming additives and fluxing agents, followed by rapid cooling to produce a solidified glass matrix [12]. The vitrification of CMSSR effectively removes organic matter and immobilizes toxic heavy metals, preventing leaching and environmental hazards, while the resulting stable vitrified slag holds promise for further applications, such as the production of cement and glass ceramics [13,14]. The glass formulation is crucial for the melting process and the properties of the glass matrix, especially with respect to viscosity and chemical durability. Viscosity is a critical parameter influencing the melting rate and homogenization of glass, with optimal performance typically achieved within the range of 1 to 10 Pa·s at the melting temperature [15-17]. Additionally, evaluating the acid leaching behavior of heavy metals from the solidified matrix is essential for assessing its environmental impact, as acidic conditions can substantially degrade the integrity of the vitrified material [18]. Despite its potential, research on the valorization of CO₂-mineralized steel slag residual through vitrification remains limited.

Therefore, this study aims to implement vitrification technology to convert CMSSR into durable glass materials. A three-component mixture comprising CMSSR,

SiO₂, and Al₂O₃ was employed to formulate waste glasses. High-temperature viscosity was measured using a rotating spindle viscometer, and a quadratic mixture model was used to predict the effects of the components on viscosity. An acid leaching test method based on China's national standard was conducted to evaluate the chemical durability of the waste glasses.

2. Experimental

2.1. Characteristics of the CO₂-mineralized steel slag residual

Ground steel slag, provided by Jiangsu Xugang Steel Group Co., Ltd. (China), was employed for CaCO₃ recovery through CO₂ mineralization, using a novel technique developed by Wang et al. [19]. During the initial leaching stage, conducted in the presence of acidic leaching agents, a Ca²⁺-rich solution was extracted for subsequent mineralization, while the resulting solid residue—designated as CMSSR—served as the target material for vitrification in this study. The crystalline phases present in the CMSSR were analyzed using X-ray diffraction (XRD) on a Bruker D8 Discover diffractometer, operated at 40 kV and 40 mA with Cu K_{α} radiation. Scanning was performed at a step size of 0.02° over a 20 range of 10° to 70°. Phase identification was carried out via JADE 6.0 software (Materials Data Inc., USA). The chemical composition of the CMSSR was analyzed via X-ray fluorescence spectrometry (XRF, Malvern Panalytical, Zetium).

2.2. Formulation and preparation of waste glasses

Based on the compositional characteristics of the CMSSR and the principle of minimal glass additives, this study aimed to develop reliable vitrification formulas by incorporating the glass formers SiO₂ and Al₂O₃. The proportions of CMSSR and glass formers were systematically varied (CMSSR: 30–100 wt%, SiO₂: 0–50 wt%, Al₂O₃: 0–25 wt%), typically in 5 wt% increments, to delineate the glass-forming region. Dry powdered CMSSR was thoroughly mixed with SiO₂ (99.5% purity) and Al₂O₃ (99.0% purity), both obtained from Sinopharm Chemical Reagent Co., Ltd. About 50 g of each fully-mixed batch was melted at 1300 °C for 1 hour in a corundum crucible under an air atmosphere. The molten mixture was then quenched onto a copper plate and allowed

to cool naturally to room temperature. The resulting glass specimens were subsequently prepared for characterization.

2.3. Characterization of waste glasses

2.3.1 Viscosity measurement

The high-temperature viscosity of the formulated waste glasses was measured using a rotary spindle viscometer (Orton RSV1600) equipped with a platinum (Pt) rotor. The rotor was immersed at a fixed depth within the molten glass and rotated at a low speed. The resulting torque was recorded and subsequently converted into viscosity values through computer-based data processing. About 200 g of powdered waste glass (150–200 µm) was placed in a 150-mL corundum crucible. The sample was then gradually heated from room temperature to the target temperature (1250–1400 °C) at a heating rate of 10 °C/min and held for 30 min. The rotor was subsequently immersed in the glass melt at a constant speed of 20 rpm, and the sample was allowed to cool at a rate of 5 °C/min from the target temperature. Throughout this cooling process, the viscosity data were recorded up to 30 Pa·s.

2.3.2 Chemical durability test

In compliance with the National Standards of the People's Republic of China—GB/T 41015–2021 (Technical Requirements for Solid Waste Vitrification Products) and GB/T 30810–2014 (Test Methods for Leachable Ions of Heavy Metals in Cement Mortar)—a mixed acid solution of sulfuric and nitric acids was prepared and used as a pH regulator for conducting heavy metal leaching tests on the vitrified glass samples. The experimental apparatus and procedure are illustrated in Fig. 1. The vitrified glass specimens were first pulverized into fine powders with particle sizes between 0.125 and 0.25 μm. Then, 10 g of this powder was added to 500 mL of deionized water and stirred with magnetic rotors at speeds ranging from 500 to 1000 rpm for 2 hours. Stirring intensity was carefully controlled to prevent excessive CO₂ absorption. The pH of the mixture was adjusted to 7.0 ± 0.5 using the acid mixture. Following the initial leaching step, the solid residues were separated from the solution via vacuum filtration using a 0.45 μm microporous membrane. These residues then underwent a second leaching process under more acidic conditions (pH 3.2 ± 0.5) with extended stirring for 7 hours.

The leachates from both stages were combined in a volumetric flask, diluted to a total volume of 2 L, and thoroughly mixed before sampling. Heavy metal concentrations in the final leachates were measured using an inductively coupled plasma atomic emission spectrometer (ICP-AES, Leeman Labs, Prodigy 7).

2.3.3 Structural analysis

A Raman spectrometer (LabRAM HR Evolution, Horiba Scientific) was used to characterize the structural evolution of the waste glasses with different SiO₂ additions. The sample preparation involved the encapsulation of homogeneous glass fragments in epoxy resin, sequential grinding to 1200-grit SiC paper, and mirror polishing via an oilbased diamond suspension. Raman spectra were recorded on optically polished glass surfaces over the spectral range of 400–1400 cm⁻¹, using a 532 nm excitation laser with a 6-s exposure time and three accumulations per sample. The spectral data were deconvoluted using the Voigt function—a convolution of Gaussian and Lorentzian profiles—through PeakFit software (version 4.12). The relative abundances of Qⁿ structural units were quantified by integrating the areas under the deconvoluted peaks, with their fractional contributions calculated based on the optimized curve fitting results [20].

3. Results and discussion

3.1. Characteristics of the CO₂-mineralized steel slag residual

Fig. 2 displays the XRD analysis of the CMSSR, and the diffraction pattern reveals the presence of ferrous oxide (FeO, PDF#75-1550), silicon oxide (SiO₂, PDF#99-0088), calcium silicate (Ca₂SiO₄, PDF#36-0642), and calcium-iron compounds (Ca₂Fe₂O₅, PDF#38-0408, and CaAl₄Fe₈O₁₉, PDF#49-1586). Both the CMSSR and the heat-treated CMSSR at 1000 °C were analyzed using X-ray fluorescence (XRF), which yielded nearly identical results. Table 1 lists the composition of the CMSSR, highlighting elevated levels of iron (Fe₂O₃: ~31 wt%), silicon (SiO₂: ~22 wt%), and calcium (CaO: ~28 wt%), alongside lower concentrations of magnesium (MgO: ~4 wt%) and aluminum (Al₂O₃: ~3 wt%). Notably, the CaO content exhibited a marked reduction of about 20 wt% compared to untreated steel slag, which typically contains around 45 wt%

CaO [21,22]. The material also demonstrated elevated concentrations of heavy metals, particularly manganese (Mn) and chromium (Cr), with Mn reaching about 6 wt%, thereby constituting a primary focus of the acid leaching investigations. The reported analytical values represent final averages derived from multiple rounds of sampling and testing.

3.2. Formulation of waste glasses

The melting experiments indicated that the green region highlighted in Fig. 3 delineates the glass-forming domain. Compositions outside this defined region did not yield glassy products, with several batches exhibiting incomplete melting. When the SiO₂ content was maintained below 20 wt%, the resultant products exhibited devitrification (blue symbols in the diagram), and they may have formed a multiphase system comprising silicates, aluminosilicate minerals, and amorphous phases. Conversely, for SiO₂ > 40 wt%, substantial unreacted residues were present (indicated by red symbols), and dark-colored aggregates formed. To determine the formulation of waste glasses, the following upper and lower compositional boundaries (in wt%) were defined: (i) CMSSR: 45~77.5 wt%, (ii) SiO₂: 22.5~40 wt%, (iii) Al₂O₃: 0~15 wt%. The density of waste glasses, measured using Archimedes' principle, increased from 2.8 to 3.3 g/cm³ with rising waste loading, with the average derived from five repeated measurements.

Based on the analysis of the glass-forming region in the CMSSR–SiO₂–Al₂O₃ waste glass system, compositions with varying waste loadings were calculated and are illustrated in Fig. 4. The primary oxide constituents—Si, Fe, Ca, and Al—exhibited substantial compositional variation across different formulations, with relative content differences reaching up to 20 wt%, significantly influencing vitrification behavior. In contrast, the concentrations of heavy metals Mn and Cr displayed relatively minor fluctuations, remaining within a 5 wt% range across all experimental batches. XRD patterns of selected waste glass samples (Fig. 5) revealed the absence of discernible crystalline diffraction peaks, confirming the predominantly amorphous nature of the solidified matrices.

3.3. The viscosity of waste glasses

As shown in the compositional diagram of the Waste–SiO₂–Al₂O₃ glass system (Fig. 3), a component-viscosity model was established using five vertices (V1–V5) and one internal point (I0). Additionally, three validation points (VP1–VP3) were selected to evaluate the model's predictive accuracy. The detailed compositions of the formulated waste glasses are listed in Table 2.

Fig. 6 illustrates the relationship between viscosity (η) and temperature (°C) for the prepared waste glasses. Glass V1, which contained the highest concentration of glass-forming additives (SiO₂ and Al₂O₃), exhibited the highest viscosity, approaching 20 Pa·s at 1300 °C. A reduction in Al₂O₃ content (V2) led to a corresponding decrease in viscosity, and a similar reduction was observed with lower SiO₂ content (VP1), indicating that diminishing glass former content effectively reduces the viscosity of the waste glasses. Notably, when the total content of glass additives was below 40 wt%, the viscosity at 1300 °C remained relatively low, consistently under 10 Pa·s. These formulations also exhibited a sharp viscosity transition between 1150 °C and 1250 °C, in contrast to the more gradual changes observed in glasses V1 and V2. Furthermore, glasses V5, I0, and V3—each containing 35 wt% additives—displayed decreasing viscosity trends with increasing SiO₂ and decreasing Al₂O₃ contents. This suggests that Al₂O₃ exerts a more pronounced effect on viscosity than SiO₂.

Fig. 7 shows the natural logarithm of viscosity (ln η) as a function of reciprocal temperature (1/T, $10^{-3} \times K^{-1}$), which exhibited a nearly linear trend. Given the simplicity and effectiveness of the Arrhenius equation in describing the viscosity-temperature relationship of waste glasses within the viscosity range of 0.4–250 Pa·s, the curves were fitted using the Arrhenius equation approximation as follows [23,24]:

$$\ln \eta = A + \frac{E}{RT} \qquad (1)$$

where A represents the temperature-independent pre-exponential factor, E denotes the activation energy of viscous flow, and R and T are the universal gas constant (8.3145 $J \cdot mol^{-1} \cdot K^{-1}$) and absolute temperature (K), respectively. Notably, the model contains only two coefficients, with E serving as the sole composition-dependent variable. The viscosity-temperature relationship can be effectively described by the Arrhenius

equation.

The viscosity typically reaches about 10 Pa·s at glass-processing temperatures that meet melt-processing constraints, with the corresponding temperature being critical for optimizing glass formulations [24]. A quantitative model relating the ternary compositions (n_i , wt%) and the temperature at which the viscosity reaches 10 Pa·s (Tv_{I0} , °C) was developed for the six waste glasses used for fitting. A partial quadratic mixture model demonstrated the best performance in fitting the Tv_{I0} data and was validated against three other verifying points. A reciprocal transformation of Tv_{I0} was applied here ($T'=1/T_{V10}$) on the basis of a final goodness of fit ($R^2=0.99$). This model takes the following general form [25,26]:

$$T' = 1/T_{V10} = \sum_{i=1}^{q} s_i n_i + selected \sum_{i=1}^{q} s_{ii} n_i^2$$
 (2)

where q is the number of components in the waste glass, s_i is the coefficient of the ith component, n_i is the weight percentage of the ith component, and s_{ii} is the coefficient for the ith component squared. The model coefficients were estimated by ordinary least squares, yielding the following values: $s_1 = 4.71902E-06$ (Waste), $s_2 = 3.30E-05$ (SiO₂), $s_3 = 1.24141E-06$ (Al₂O₃), $s_{22} = -5.10561E-07$ (SiO₂*SiO₂), and $s_{11} = s_{33} = 0$.

Fig. 8 compares the predicted and measured T_{VI0} values, demonstrating strong agreement between the two and indicating that the partial quadratic mixture model effectively captures the relationship between T_{VI0} and the compositional variables. Although the model shows a minor tendency to overestimate T_{VI0} , the maximum deviation is limited to 2.1%. A three-dimensional diagram generated by the model (Fig. 9) illustrates the relationship between the compositional components and T_{VI0} within the Waste–SiO₂–Al₂O₃ ternary system, clearly visualizing the temperature at which the viscosity reaches 10 Pa·s and the influence of each component. Additionally, the color-coded contour lines at the base of the diagram represent T_{VI0} isopleths within the experimental domain. The plot indicates that reducing the total additive content generally leads to a decrease in T_{VI0} , with Al₂O₃ exerting a more pronounced influence than SiO₂, consistent with the trends observed in Fig. 6. The quantitative compositional effects on T_{VI0} derived from the partial quadratic mixture model provide useful

guidance for optimizing waste glass formulations compatible with current vitrification processes.

3.4. Chemical durability of waste glasses

Fig. 10a illustrates the concentrations of total Cr and Mn ions in the leachates derived from acid leaching tests on 22 waste glass samples situated within the glass-forming region. For all tested compositions, the concentration of Cr released was consistently below 0.02 mg/L, substantially lower than the regulatory threshold of 0.2 mg/L stipulated by the Chinese standards for vitrified solid waste products. Additionally, the maximum leaching concentration of Mn was about 0.7 mg/L, which is also below the permissible limit of 1.0 mg/L established by the national standard. This indicates the excellent chemical durability of the formulated waste glasses, highlighting their potential for treating the CMSSR and effectively capturing these heavy metals.

In summary, the leaching of Cr from these waste glasses in acidic environments is minimal, probably due to its low percentage of waste (~0.3 wt%), which decreases the potential for leaching. Consequently, Mn, which has relatively high leaching concentrations, is the element of primary concern in this study. Further data analysis revealed that as the SiO₂ content increased, the leaching concentration of Mn generally decreased, indicating the enhanced chemical stability of the waste glasses, as illustrated in Fig. 10b.

3.5 Structure analysis of waste glasses

Raman spectroscopy has emerged as a powerful analytical tool for probing glass network structures and is directly correlated with future chemical durability and heavy metal immobilization efficiency in vitrified waste forms [27]. Three samples with increasing SiO₂ additions (22.5, 30, and 40 wt%) and a fixed Al₂O₃ addition (5 wt%) were subjected to Raman spectroscopy analysis (designated AS22.5 to AS40, corresponding to 22.5–40 wt% SiO₂ additions), and the results are shown in Fig. 11. The spectral evolution observed in the 800–1200 cm⁻¹ region reveals characteristic Si-O stretching vibrations, with distinct bands centered at 860, 920, 980, and 1050 cm⁻¹ corresponding to specific Si-O tetrahedral units denoted as Qⁿ (where Q represents a

silica tetrahedron and n indicates the number of bridging oxygen atoms, ranging from 0 to 3) [28,29]. The spectra were deconvoluted using Voigt profiles associated with Q^0 , Q^1 , Q^2 , and Q^3 species, as illustrated in Fig. 11a. The relative proportions of these units as a function of SiO₂ content are presented in Fig. 11b. It is evident that the fraction of Q^0 units decreases progressively with increasing SiO₂ addition, while the proportion of Q^3 units increases, indicating enhanced polymerization of the silica network structure as the SiO₂ content rises.

The ratio of non-bridging oxygen to total oxygen (NBO/T) reflects the degree of depolymerization (DOP) of the glass network structure. The DOP is determined using the following equation [20]:

$$NBO/T = 4 \times Q^{0} + 3 \times Q^{1} + 2 \times Q^{2} + 3 \times Q^{1} + 0 \times Q^{4}$$
(3)

The calculation results of the DOP values are presented in Fig. 11c, which shows that the DOP increases from 2.04 to 2.35 as the SiO₂ addition decreases from 40 to 22.5 wt%, indicating an increase in non-bridging oxygens and depolymerization of the glass network. This behavior is attributed to the relatively high CaO concentration in the original CMSSR, where CaO acts as a network modifier, decomposing the [SiO₄] network structure based on the formation of less stable Si-O-Ca bonds [18,30]. This promotes the migration of ions, thereby increasing the extent of Mn leaching. An increase in the proportion of SiO₂ added improved the chemical durability of the waste glass, leading to a reduction in the leaching of Mn ions.

4. Conclusion

This work investigated the vitrification of CO₂-mineralized steel slag residuals through the incorporation of silica and alumina. A representative subset of glass formulations was selected to investigate their high-temperature viscosity, and a quadratic mixture model was used to effectively correlate the component and the temperature at which the viscosity reached 10 Pa·s. The leaching performance of heavy metals was evaluated through acid leaching tests in accordance with Chinese national standards, while Raman spectroscopy was employed to investigate the influence of

SiO₂ content on the structural configuration of the glasses and its correlation with Mn immobilization efficiency. The key findings are summarized as follows:

- (1) Ternary CMSSR–SiO₂–Al₂O₃ glasses were successfully synthesized at a melting temperature of 1300 °C. The glass-forming region was delineated within the compositional boundaries of 45–77.5 wt% CMSSR, 22.5–40 wt% SiO₂, and 0–15 wt% Al₂O₃.
 - (2) The optimal mixture model is expressed as follows:

$$T' = 1/T_{V10} = \sum_{i=1}^{q} s_i n_i + selected \sum_{i=1}^{q} s_{ii} n_i^2$$

 $s_1 = 4.71902E - 06$, $s_2 = 3.30E - 05$, $s_3 = 1.24141E - 06$, $s_{22} = -5.10561E - 07$, $s_{11} = s_{33} = 0$.

A 3D plot based on this model illustrates the impact of the ternary composition on the melting temperature. A reduction in the silica and alumina additives resulted in a lower glass viscosity.

(3) The highest observed leaching concentrations for Cr and Mn were below $0.02\,\text{mg/L}$ and $0.7\,\text{mg/L}$, respectively, fully meeting the regulatory limits prescribed by China's standards for vitrified solid waste products (Cr $\leq 0.2\,\text{mg/L}$, Mn $\leq 1.0\,\text{mg/L}$). These findings underscore the superior chemical stability of the developed glass matrices. Moreover, increasing the SiO₂ content led to greater polymerization within the glass network, which enhanced its chemical resistance and effectively minimized Mn release.

Acknowledgements

This work was supported by the Hubei Provincial Key Research Projects (No. 2022BCA070).

References

- [1] W. Gao, W. Zhou, X. Lyu, X. Liu, H. Su, C. Li, H. Wang, Comprehensive utilization of steel slag: A review, Powder Technol. 422 (2023) 118449, https://doi.org/10.1016/j.powtec.2023.118449.
- [2] J. Guo, Y. Bao, M. Wang, Steel slag in China: Treatment, recycling, and management, Waste Manag. 78 (2018) 318–330, https://doi.org/10.1016/j.wasman.2018.04.045.
- [3] Y. Jiang, T. Ling, C. Shi, S. Pan, Characteristics of steel slags and their use in cement and concrete—A review, Resour. Conserv. Recycl. 136 (2018) 187–197, https://doi.org/10.1016/j.resconrec.2018.04.023.
- [4] L. Yang, T. Wei, S. Li, Y. Lv, T. Miki, L. Yang, T. Nagasaka, Immobilization persistence of Cu, Cr, Pb, Zn ions by the addition of steel slag in acidic contaminated mine soil, J. Hazard. Mater. 412 (2021) 125176, https://doi.org/10.1016/j.jhazmat.2021.125176.
- [5] Q. Dong, G. Wang, X. Chen, J. Tan, X. Gu, Recycling of steel slag aggregate in portland cement concrete: An overview, J. Clean. Prod. 282 (2021) 124447, https://doi.org/10.1016/j.jclepro.2020.124447.
- [6] Y. Guo, J. Xie, J. Zhao, K. Zuo, Utilization of unprocessed steel slag as fine aggregate in normal-and high-strength concrete, Constr. Build. Mater. 204 (2019) 41–49, https://doi.org/10.1016/j.conbuildmat.2019.01.178.
- [7] G. Wang, X. Chen, Q. Dong, J. Yuan, Q. Hong, Mechanical performance study of pervious concrete using steel slag aggregate through laboratory tests and numerical simulation, J. Clean. Prod. 262 (2020) 121208, https://doi.org/10.1016/j.jclepro.2020.121208.
- [8] A. Sanna, M. Uibu, G. Caramanna, R. Kuusik, M.M. Maroto-Valer, A review of mineral carbonation technologies to sequester CO₂, Chem. Soc. Rev. 43.23 (2014) 8049–8080, https://doi.org/10.1039/C4CS00035H.
- [9] A. Said, T. Laukkanen, M. Järvinen, Pilot-scale experimental work on carbon dioxide sequestration using steelmaking slag, Appl. Energy. 177 (2016) 602–611, https://doi.org/10.1016/j.apenergy.2016.05.136.

- [10] A.L.V. Cubas, M. de Medeiros Machado, M. de Medeiros Machado, F. Gross, R.F. Magnago, E.H.S. Moecke, I. Gonçalvez de Souza, Inertization of heavy metals present in galvanic sludge by DC thermal plasma, Environ. Sci. Technol. 48.5 (2014) 2853–2861, https://doi.org/10.1021/es404296x.
- [11] A.L.V. Cubas, M. de Medeiros Machado, M. de Medeiros Machado, A.R. de Aguiar Dutra, E.H.S. Moecke, H.D. Fiedler, P. Bueno, Final treatment of spent batteries by thermal plasma, J. Environ. Manage. 159 (2015) 202–208, https://doi.org/10.1016/j.jenvman.2015.05.004.
- [12] R.C. Sanito, M. Bernuy-Zumaeta, S.J. You, Y. Wang, A review on vitrification technologies of hazardous waste, J. Environ. Manage. 316 (2022) 115243, https://doi.org/10.1016/j.jenvman.2022.115243.
- [13]S. Wu, S. Zhang, Y. Zhang, C. Gao, Reuse of vitrified argon oxygen decarburization slag as supplementary cementitious materials: Comprehensive performance and chromium immobilization mechanism, Constr. Build. Mater. 348 (2022) 128647, https://doi.org/10.1016/j.conbuildmat.2022.128647.
- [14] Y. Long, Y. Song, H. Huang, Y. Yang, D. Shen, H. Geng, J. Ruan, F. Gu, Preparation of foam glass ceramics from hazardous waste vitrification slag with the addition of Na₂CO₃, Constr. Build. Mater. 404 (2023) 133225, https://doi.org/10.1016/j.conbuildmat.2023.133225.
- [15] G. Fang, C. Liu, K. Li, K. Xu, X. Zhao, Vitrification of nuclear-contaminated HEPA filter media: A study on the viscosity-component correlation and the volatilization of simulated radionuclides, J. Non-Cryst. Solids. 619 (2023) 122568, https://doi.org/10.1016/j.jnoncrysol.2023.122568.
- [16] P. Ferkl, P. Hrma, A. Kruger, Parsimonious viscosity-composition relationships for high-temperature multicomponent glass melts, J. Asian Ceram. Soc. 10 (2022) 83– 98, https://doi.org/10.1080/21870764.2021.2012903.
- [17] P. Hrma, B.M. Arrigoni, M.J. Schweiger, Viscosity of many-component glasses, J. Non-Cryst. Solids. 355 (2009) 891–902, https://doi.org/10.1016/j.jnoncrysol.2009.03.005.

- [18] W. Song, Z. Zhu, J. Cao, Z. Wang, Y. Chang, Z. Wang, The effect of sulfur on the leaching of Cr³⁺, Cr⁶⁺, Pb²⁺ and Zn²⁺ from fly ash glass, Chemosphere. 305 (2022) 135387, https://doi.org/10.1016/j.chemosphere.2022.135387.
- [19]Y. Wang, X. Zheng, Y. Wang, S. Lu, Z. Fei, J. Li, L. Ji, S. Yan, Fate of Ca²⁺ and metal impurities of a typical coal fly ash in amino acid mediated CO₂ mineralization and simultaneous CaCO₃ recovery, Sep. Purif. Technol. 353 (2025) 128610, https://doi.org/10.1016/j.seppur.2024.128610.
- [20] L. Deng, B. Yao, W. Lu, M. Zhang, H. Li, H. Chen, M. Zhao, Y. Du, M. Zhang, Y. Ma, W. Wang, Effect of SiO₂/Al₂O₃ ratio on the crystallization and heavy metal Immobilization of glass ceramics derived from stainless steel slag, J. Non-Cryst. Solids. 593 (2022) 121770, https://doi.org/10.1016/j.jnoncrysol.2022.121770.
- [21]X. Cheng, W. Tian, Q. Yuan, W. Chen, J. Wan, J. Guo, J. Cai, Effect of carbon dioxide mineralization curing on mechanical properties and microstructure of Portland cement-steel slag-granulated blast furnace slag ternary paste, Constr. Build. Mater. 431 (2024) 136553, https://doi.org/10.1016/j.conbuildmat.2024.136553.
- [22] K. Wang, C. Qian, R. Wang. The properties and mechanism of microbial mineralized steel slag bricks, Constr. Build. Mater. 113 (2016) 815-823, https://doi.org/10.1016/j.conbuildmat.2016.03.122.
- [23] P. Hrma, Arrhenius model for high-temperature glass-viscosity with a constant preexponential factor, J. Non-Cryst. Solids. 354 (2008) 1962-1968, https://doi.org/10.1016/j.jnoncrysol.2007.11.016.
- [24] P. Hrma, S.S. Han, Effect of glass composition on activation energy of viscosity in glass-melting-temperature range, J. Non-Cryst. Solids. 358 (2012) 1818-1829, https://doi.org/10.1016/j.jnoncrysol.2012.05.030.
- [25] G.F. Piepel, J.W. Shade, In situ vitrification and the effects of soil additives-a mixture experiment case study, J. Am. Ceram. Soc. 75 (1992) 112–116, https://www.researchgate.net/publication/318447223.
- [26] J.D. Vienna, D.S. Kim, I.S. Muller, G.F. Piepel, A.A. Kruger, Toward understanding the effect of low-activity waste glass composition on sulfur

- solubility, J. Am. Ceram. Soc. 97 (2014) 3135–3142, https://doi.org/10.1111/jace.13125.
- [27] Z. Luo, F. He, W. Zhang, Y. Xiao, J. Xie, R. Sun, M. Xie, Effects of fluoride content on structure and properties of steel slag glass-ceramics, Mater. Chem. Phys. 242 (2020) 122531, https://doi.org/10.1016/j.matchemphys.2019.122531.
- [28] Z. Wang, C. Liu, G. Fang, P. Lin, K. Li, L. Li, K. Xu, Vitrification of nuclear contaminated lead-boron polyethylene, J. Non-Cryst. Solids. 564 (2021) 120832, https://doi.org/10.1016/j.jnoncrysol.2021.120832.
- [29] Z. Jia, C. Liu, C. Niu, K. Li, K. Xu, Volatilization of sodium and boron from nuclear waste glass and associated effects on glass structure and thermal stability, J. Nucl. Mater. 587 (2023) 154712, https://doi.org/10.1016/j.jnucmat.2023.154712.
- [30] W. Song, J. Cao, Z. Wang, X. Geng, J. Lu, Glass-ceramics microstructure formation mechanism for simultaneous solidification of chromium and nickel from disassembled waste battery and chromium slag, J. Hazard. Mater. 403 (2021) 123598, https://doi.org/10.1016/j.jhazmat.2020.123598.

Table 1 Chemical composition of the residual steel slag obtained from XRF analysis.

Composition	wt%
Fe ₂ O ₃	31.02
CaO	28.27
SiO_2	22.29
MnO	5.75
MgO	4.30
Al_2O_3	3.20
P_2O_5	2.64
SO_3	0.94
TiO ₂	0.92
Cr ₂ O ₃	0.29
V_2O_5	0.20
Na ₂ O	0.18
SUM	100.00

Table 2 Composition of the formulated waste glasses.

Type of points	Code	Waste (wt%)	SiO ₂ (wt%)	Al ₂ O ₃ (wt%)
Vertices	V1	45.00	40.00	15.00
	V2	55.00	40.00	5.00
	V3	65.00	35.00	0.00
	V4	77.50	22.50	0.00
	V5	65.00	22.50	12.50
Internal point	10	65.00	30.00	5.00
Verifying	VP1	60.00	25.00	15.00
points	VP2	70.00	25.00	5.00
	VP3	75.00	25.00	0.00

Figure Captions

- Fig. 1 Experimental setup and procedure for the acid leaching test.
- Fig. 2 XRD pattern of the CO₂-mineralized steel slag.
- Fig. 3 Experimental region of the Waste–SiO₂–Al₂O₃ waste glass.
- Fig. 4 Calculated compositions of waste glasses with various waste loadings.
- Fig. 5 XRD patterns of the waste glass samples (only partially displayed).
- Fig. 6 Viscosity as a function of temperature for glasses V1–V5, I0, and VP1–VP3.
- Fig. 7 ln η as a function of 1/T (10⁻³×K⁻¹) for glasses V1–V5, I0, and VP1–VP3.
- **Fig. 8** Comparison of the predicted T_{V10} and measured T_{V10} . RMSE: Root mean square error.
- **Fig. 9** 3D diagram correlating the components and Tv_{10} .
- **Fig. 10** (a) Leaching concentrations of total Cr and Mn ions from waste glasses and (b) effect of the addition of SiO₂ on the leaching of Mn. Lines have been added for easy visual guidance.
- **Fig. 11** (a) Deconvolution of the Raman spectral region between 800 cm⁻¹ and 1200 cm⁻¹ in the AS22.5, AS30 and AS40 glasses, (b) the proportion of Qⁿ from deconvolution results versus SiO₂ addition, and (c) the calculation of NBO/T.

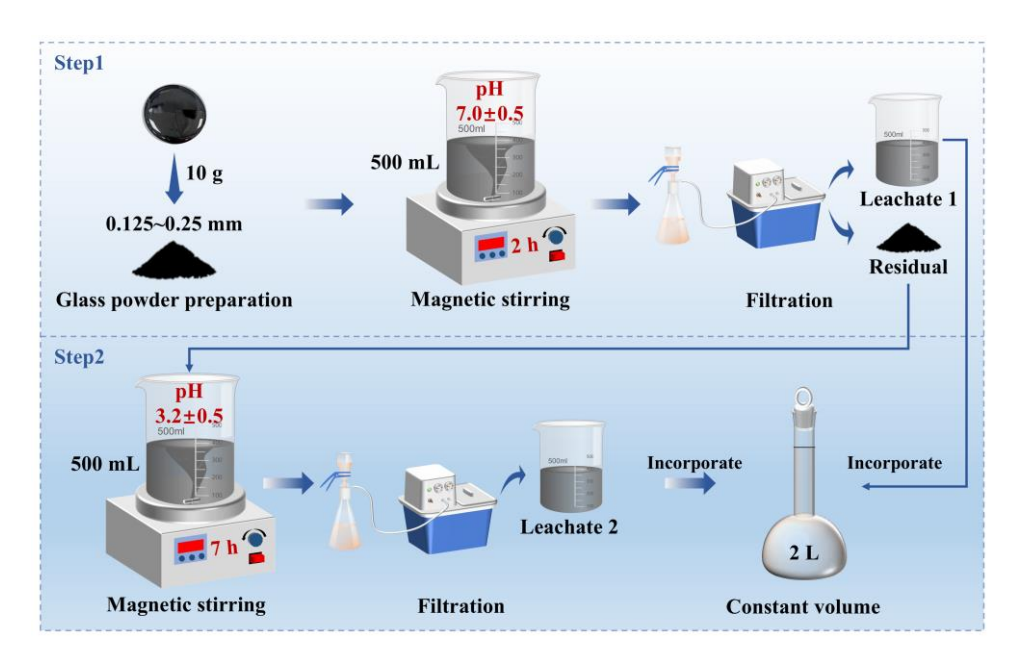


Fig. 1

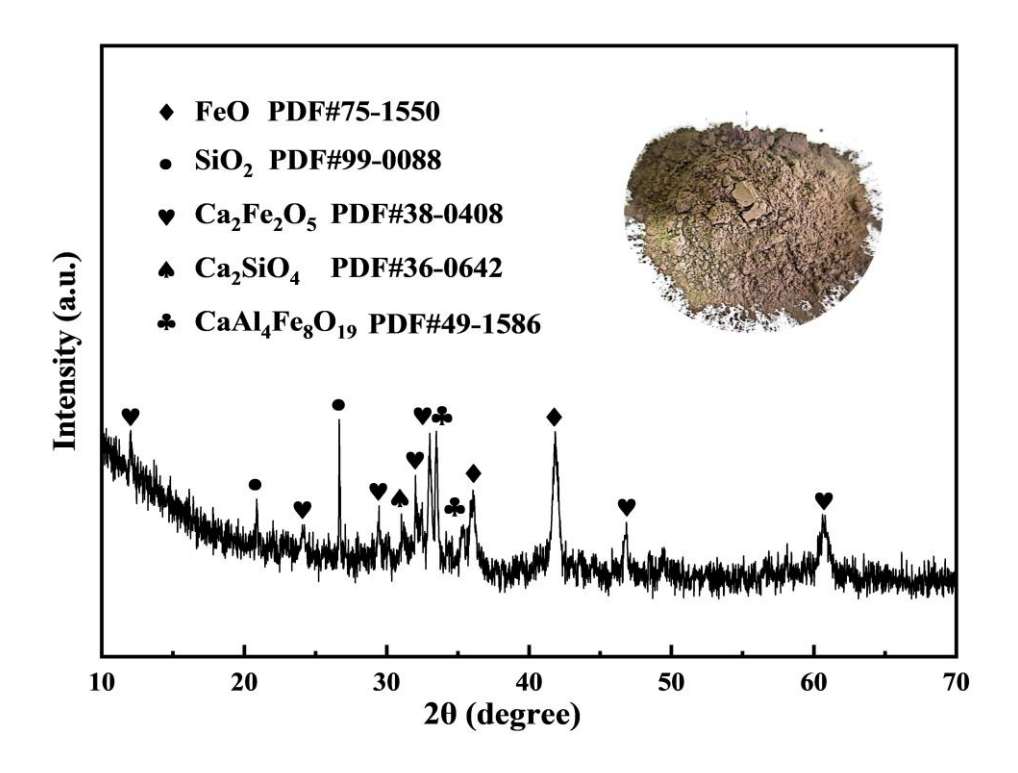


Fig. 2

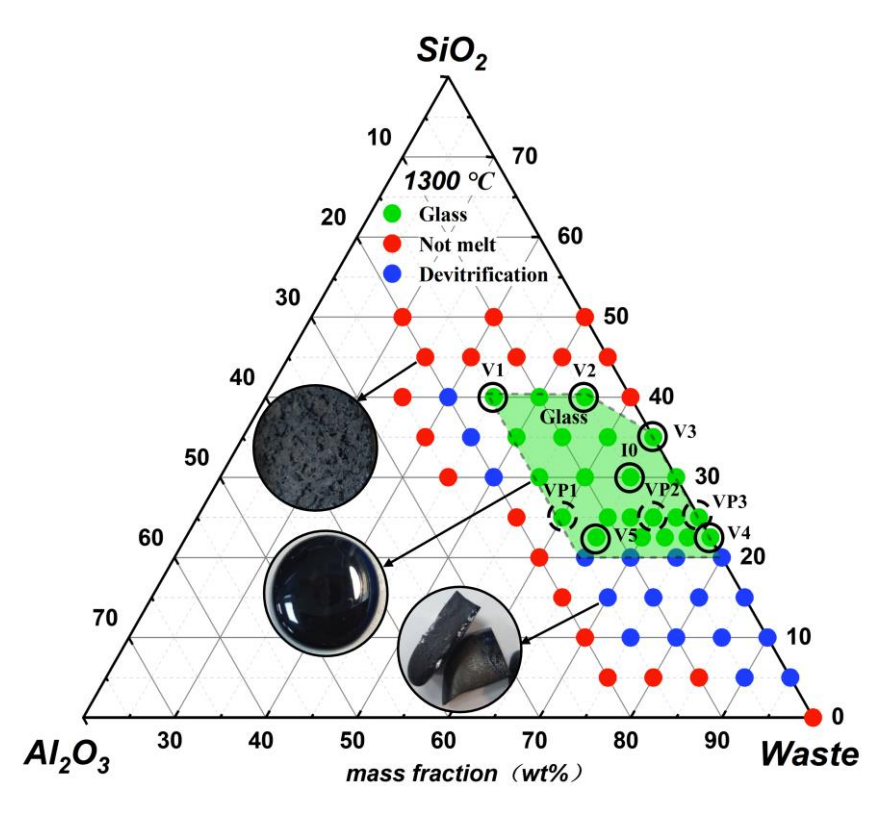


Fig. 3

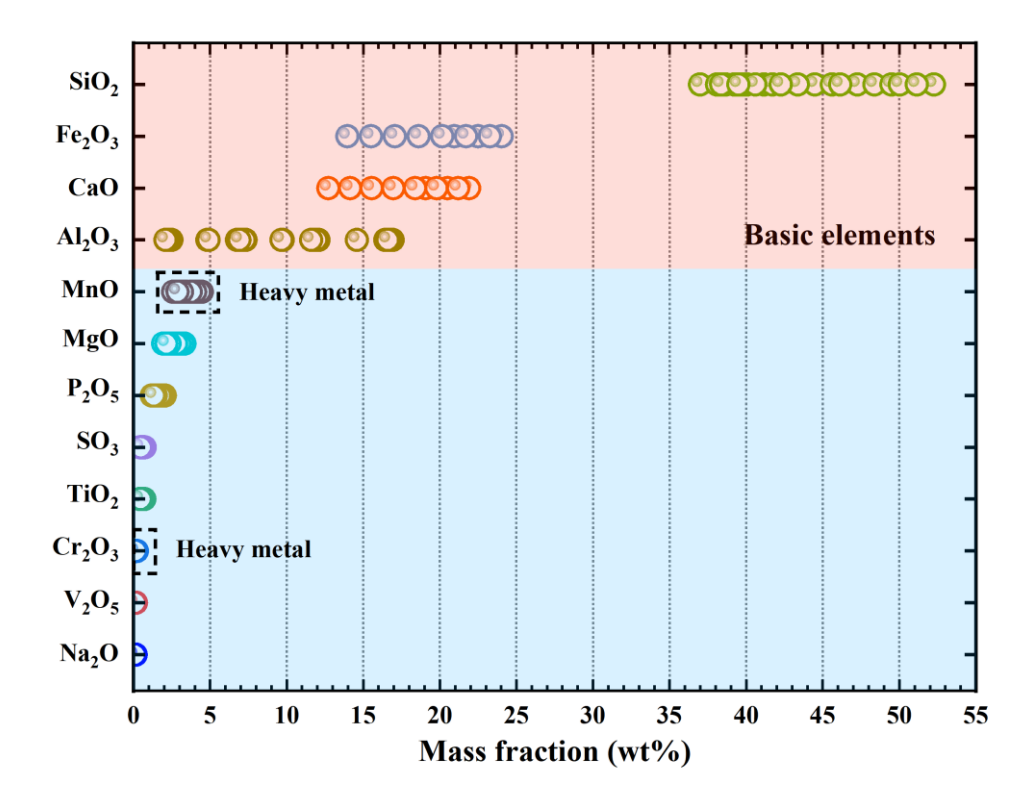


Fig. 4

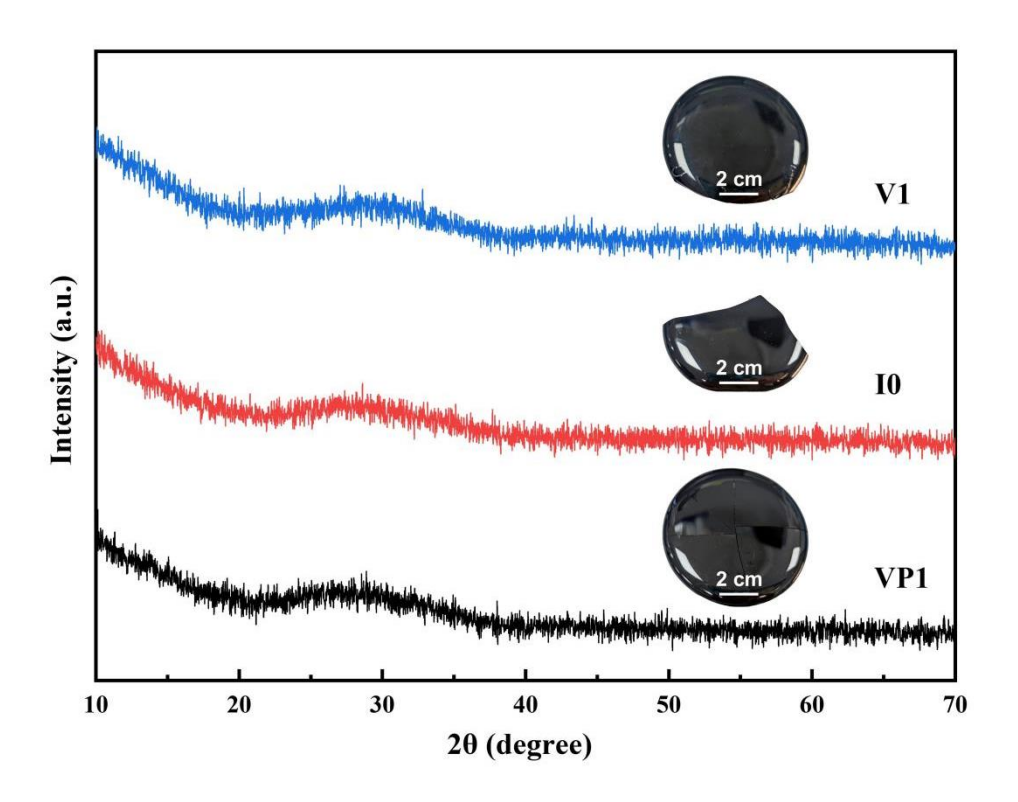


Fig. 5

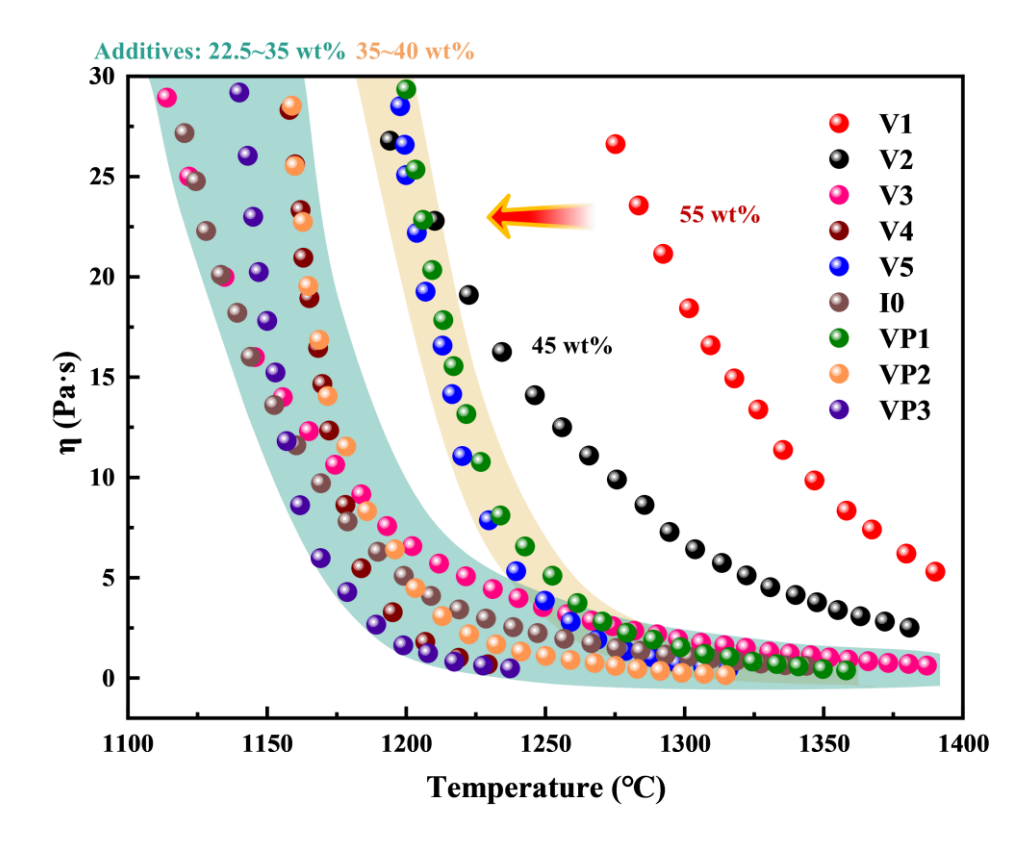


Fig. 6

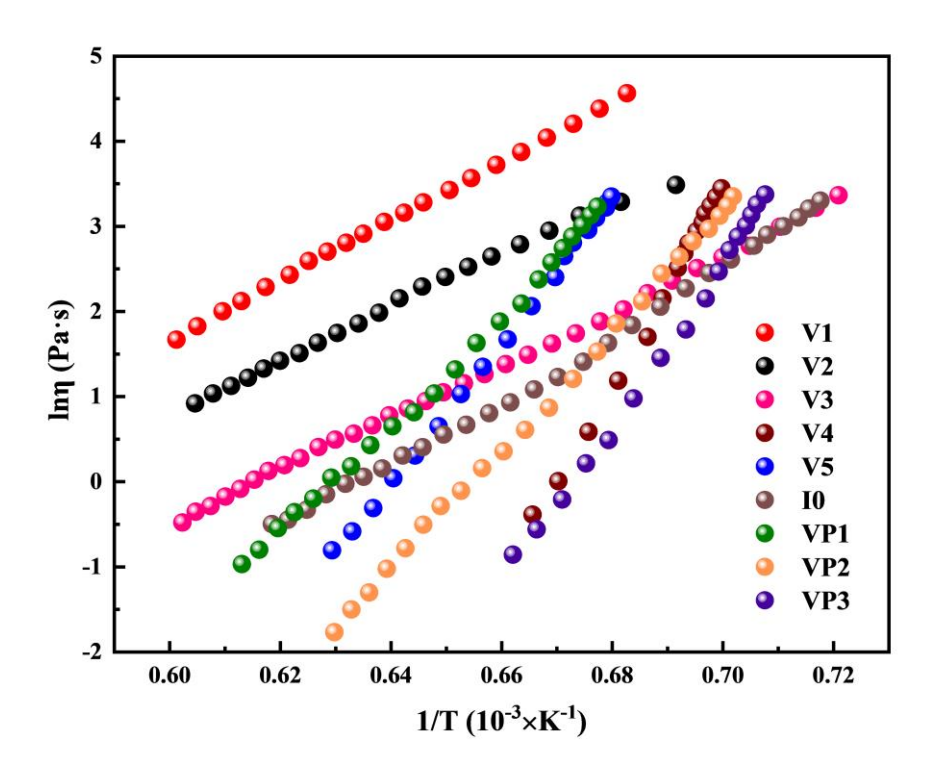


Fig. 7

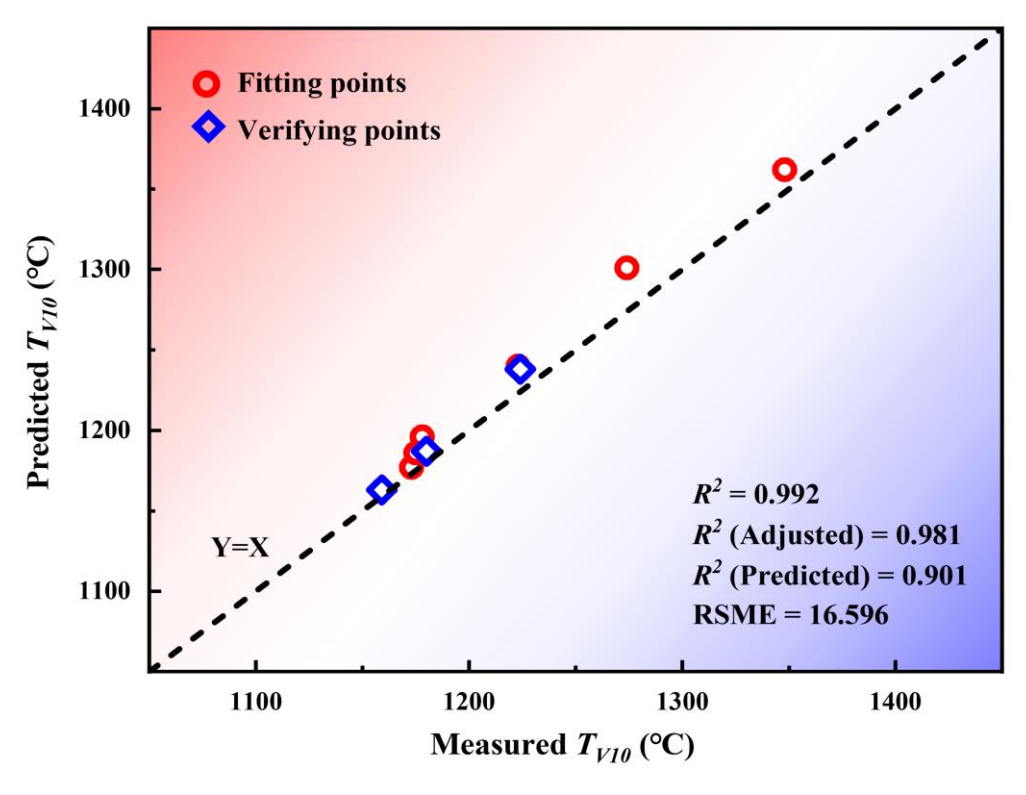


Fig. 8

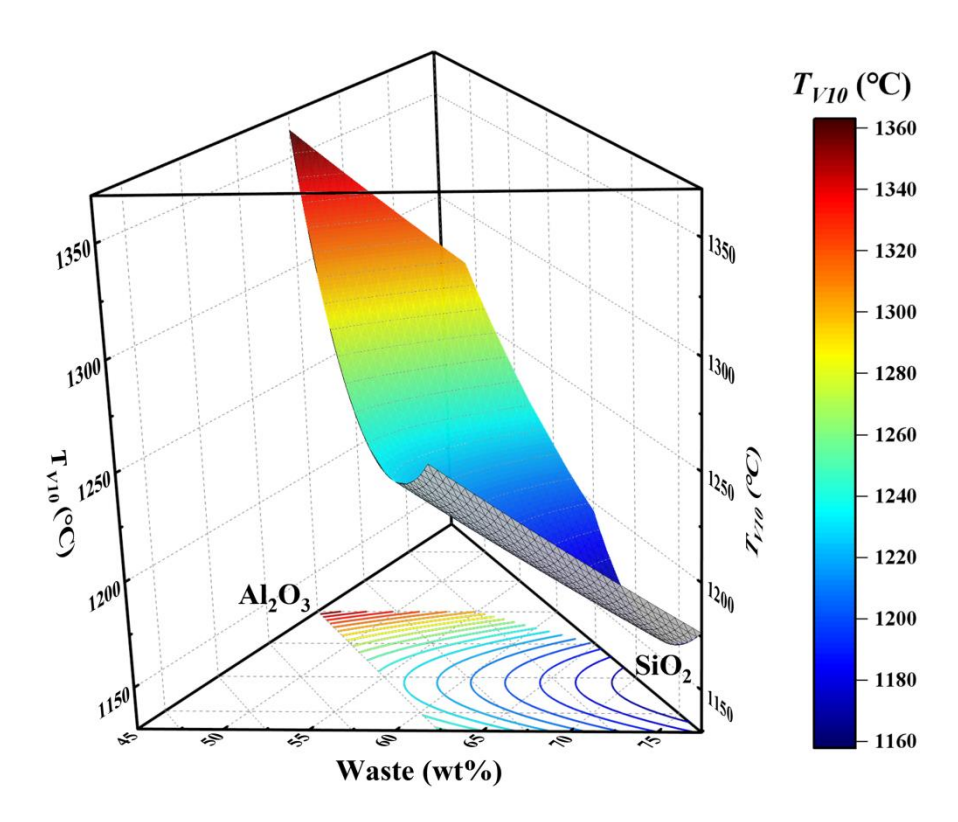


Fig. 9

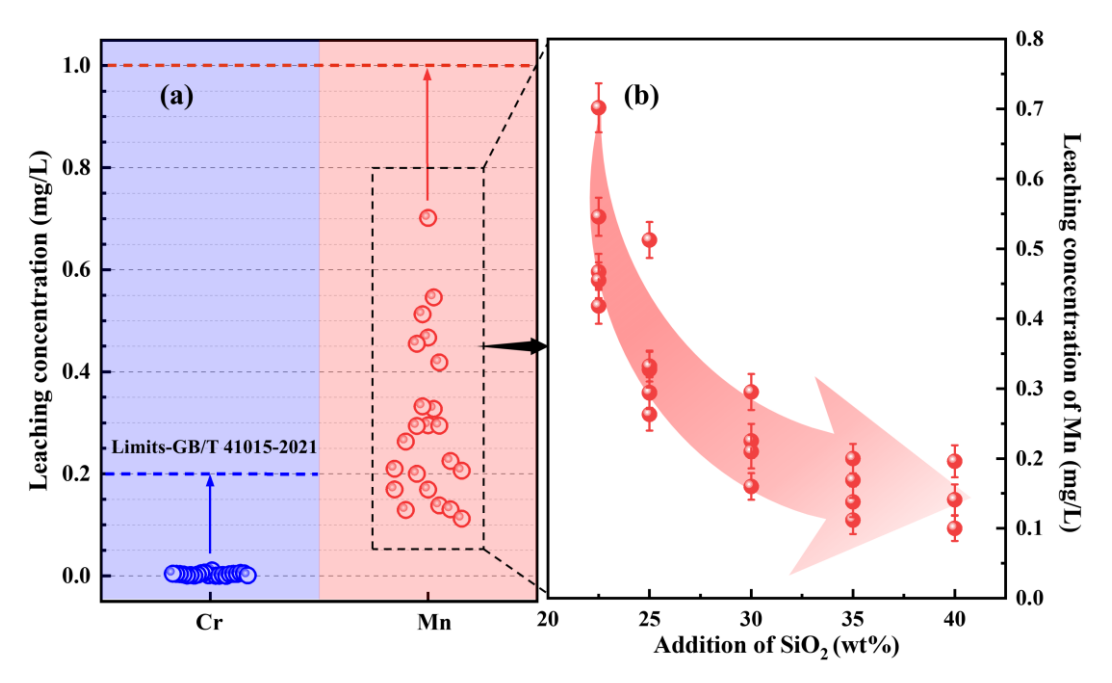


Fig. 10

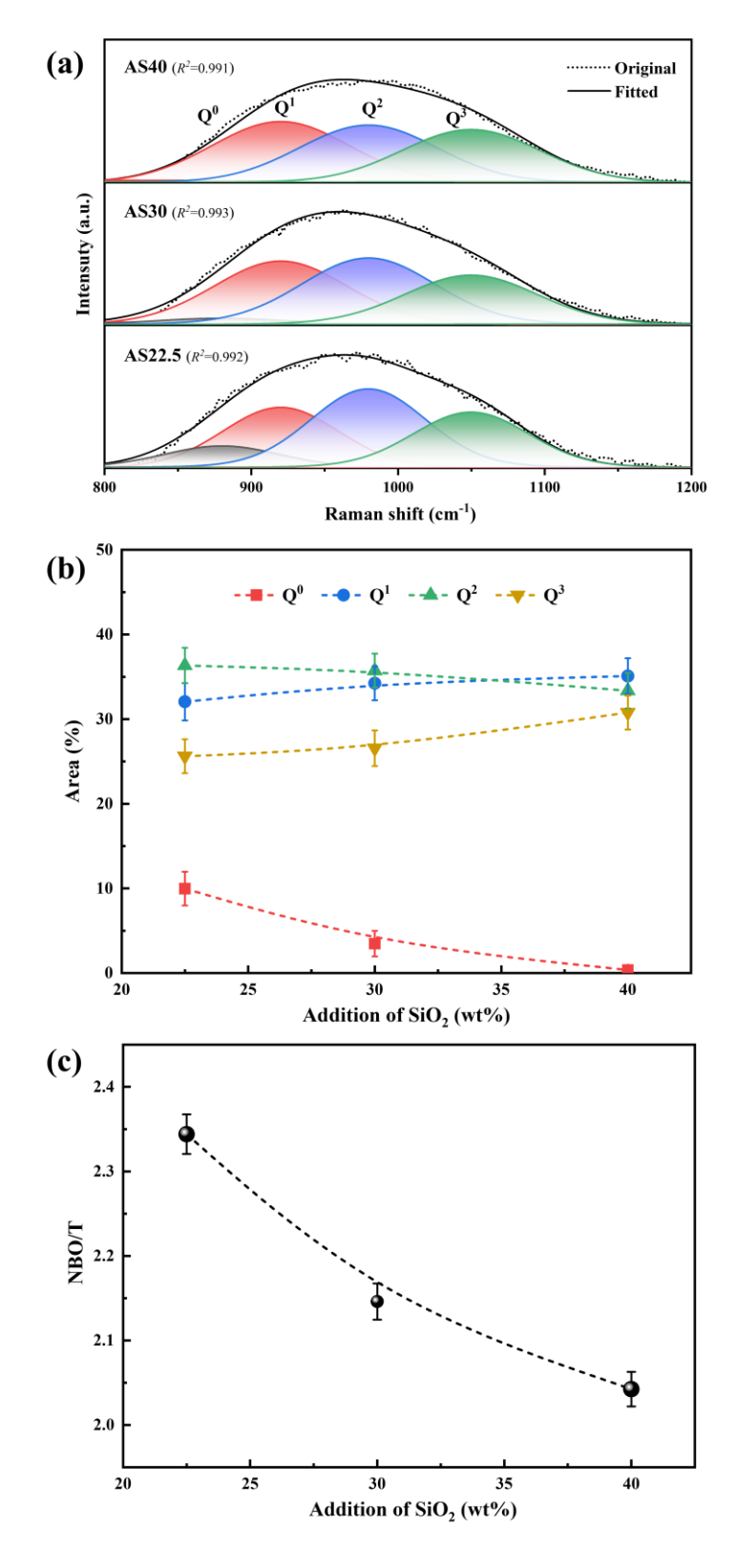


Fig. 11